

Mechanically-stacked Perovskite/CIGS Tandem Solar Cells with Efficiency of 23.9% and Reduced Oxygen Sensitivity

Heping Shen,^{1,*} The Duong,¹ Jun Peng,¹ Daniel Jacobs,¹ Nandi Wu,¹ Junbo Gong,² Yiliang Wu,¹ Siva Krishna Karuturi,³ Xiao Fu,¹ Klaus Weber,¹ Xudong Xiao,² Thomas P. White,¹ Kylie Catchpole¹

¹Centre for Sustainable Energy Systems, Research School of Engineering, The Australian National University, Canberra 2601, Australia

²Department of Physics, The Chinese University of Hong Kong, Shatin, New Territory, Hong Kong, China

³Department of Electronic Materials Engineering Research School of Physics and Engineering, The Australian National University, Canberra, ACT 2601, Australia.

* Corresponding author: heping.shen@anu.edu.au;

Figure S1 shows the reverse and forward scanning J - V curves of the opaque solar cells based on the quadruple cation perovskite ($\text{Cs}_{0.05}\text{Rb}_{0.05}\text{FA}_{0.765}\text{MA}_{0.135}\text{PbI}_{2.55}\text{Br}_{0.45}$) with a bandgap of around 1.62 eV. Almost no hysteresis was observed at a slow scanning rate of 50mV/s. Each scanning is performed after the device reached equilibrium at open-circuit condition. The steady-state efficiency is also in good agreement with the J - V scanning, reaching 20.0% at V_{mpp} of 0.95V.

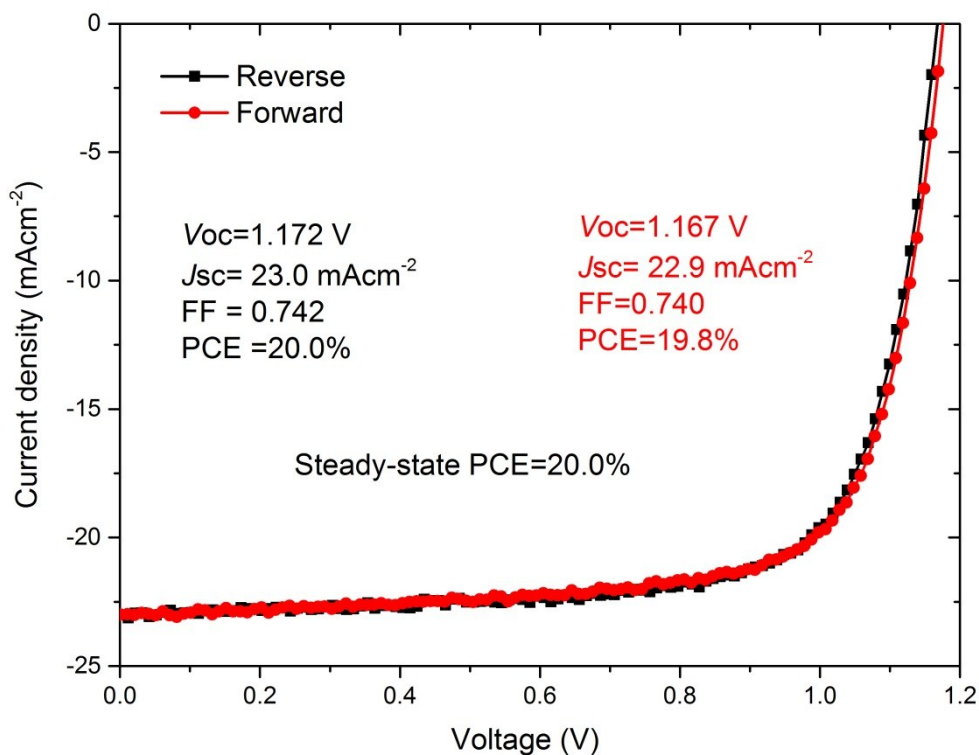


Figure S1. Photovoltaic performance of the opaque PSCs (both reverse and forward scanning at a scanning rate of 50mV/s) based on $\text{Cs}_{0.05}\text{Rb}_{0.05}\text{FA}_{0.765}\text{MA}_{0.135}\text{PbI}_{2.55}\text{Br}_{0.45}$.

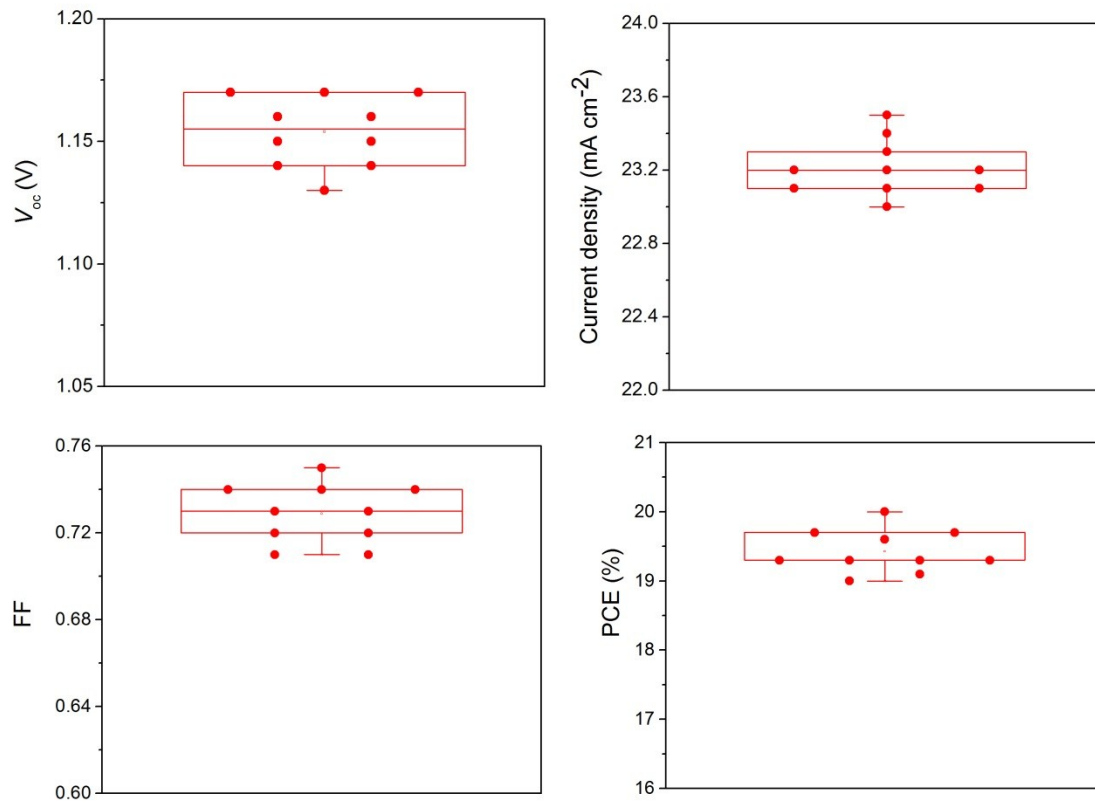


Figure S2. Photovoltaic metrics of ten normal bandgap opaque solar cells from two batches based on $\text{Cs}_{0.05}\text{Rb}_{0.05}\text{FA}_{0.765}\text{MA}_{0.135}\text{PbI}_{2.55}\text{Br}_{0.45}$. The average and standard deviation of each photovoltaic parameter are V_{oc} : 1.154 ± 0.014 V; J_{sc} : 23.21 ± 0.15 mA cm^{-2} ; FF: 0.729 ± 0.014 ; PCE: $19.43 \pm 0.31\%$

With the same device structure, opaque cells based on MAPbI₃ show lower photovoltaic performance than that based on the quadruple perovskite (Fig.S1), especially in terms of V_{oc} . Similarly, the device shows negligible hysteresis behaviour. The steady-state efficiency reaches 17%.

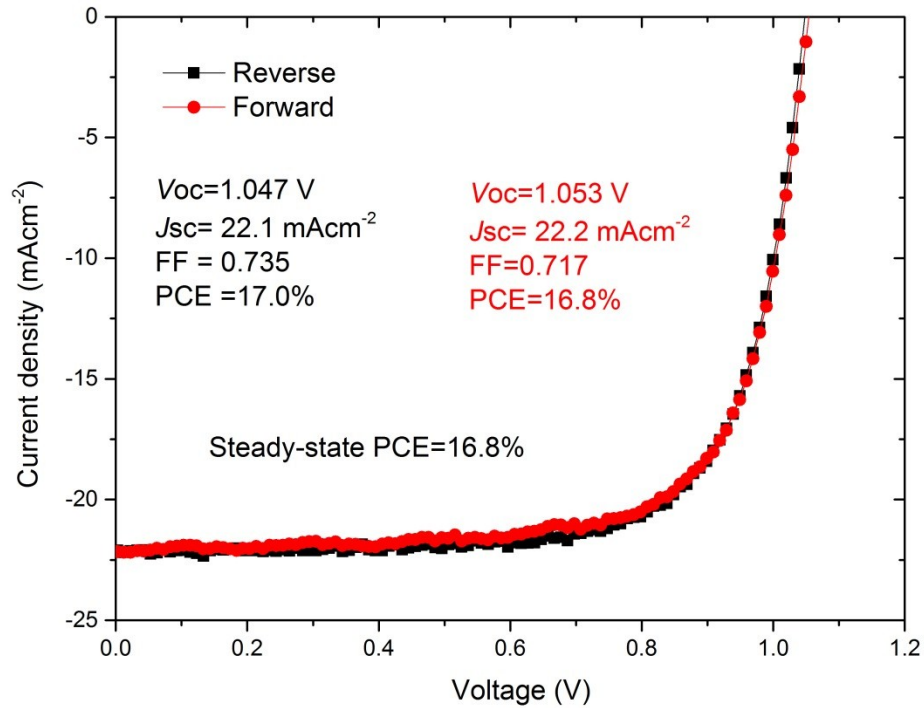


Figure S3. Photovoltaic performance of the opaque PSCs based on MAPbI₃ (both reverse and forward scanning under a scanning rate of 50 mV/s)

Optical management results by employing the texture foil on the front surface and MgF_2 anti-reflection film on the rear side for the PSC based on $\text{Cs}_{0.05}\text{Rb}_{0.05}\text{FA}_{0.765}\text{MA}_{0.135}\text{PbI}_{2.55}\text{Br}_{0.45}$ are shown in Figure S4. The effect of 180 nm MgF_2 on the reflectance mostly occurs in the long wavelength region from ~ 800 nm-1200 nm, which is very slight for the perovskite solar cell. The current density difference of the normal bandgap semi-transparent solar cell with and without MgF_2 is only around 0.3 mAcm^{-2} , corresponding to relative change of around 1%. The reflectance peak (~ 1000 nm, black line) in the reflection film is red-shifted to nearly 1100nm. The textured foil reduced the reflectance in the entire wavelength range.

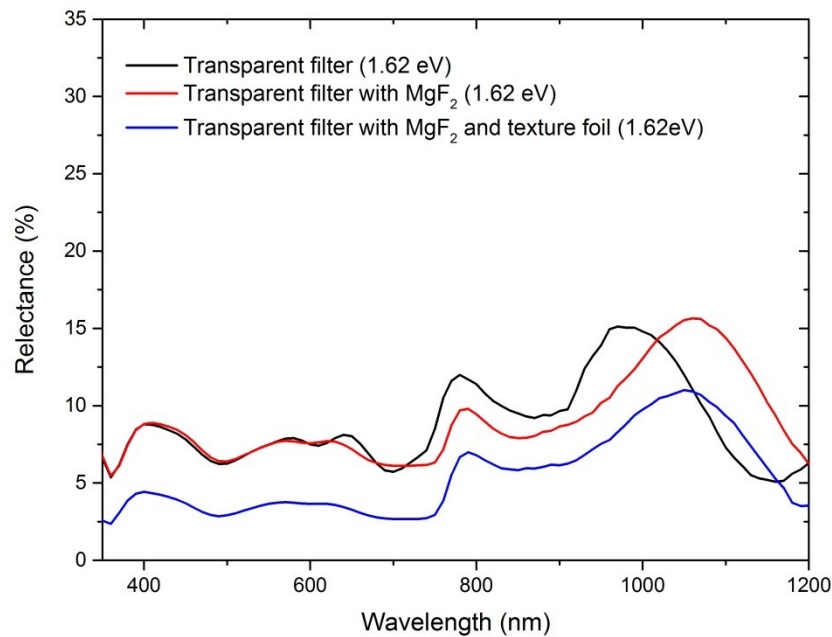


Figure S4. Reflectance of the transparent filters based on the normal bandgap perovskite ($\text{Cs}_{0.05}\text{Rb}_{0.05}\text{FA}_{0.765}\text{MA}_{0.135}\text{PbI}_{2.55}\text{Br}_{0.45}$) by incorporating MgF_2 on the rear side and textured foil on the front side

To tune the high bandgap perovskite composition, the effect of Cs doping and Rb doping were verified. As is shown, we found that FA/MA based sample (black line), both yellow phase (non-perovskite, noted as δ) and the excess PbI_2 peak (noted as $\#$) were observable. With Rb doping (red line), the PbI_2 peak was inhibited completely, while the yellow phase still exists. In the meantime, an additional Rb-phase (noted as σ) appears. To further remove these two unfavourable phases, Cs doping is effective. By increasing the Cs doping from 5% to 10% and 15%, the two peaks are effectively reduced. 10% Cs doping is optimal, and higher Cs doping (15%) induces Rb-rich perovskite phase.

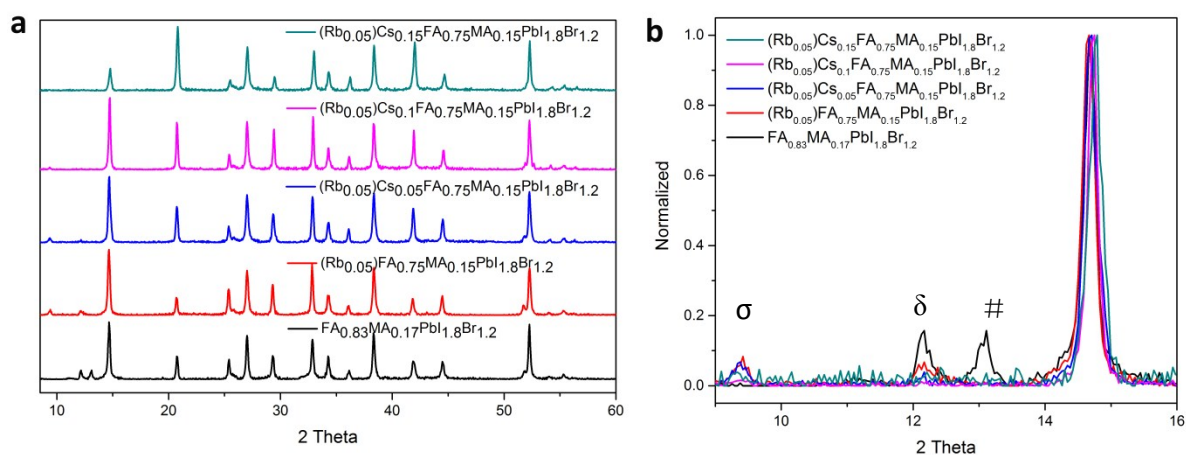


Figure S5. XRD patterns of high bandgap perovskite (~ 1.75 eV) without Cs doping and with Cs doping

To check whether 5% Rb is optimal, we varied the doping concentration from 0% to 7.5%, found that too much Rb results in Rb-rich perovskite phase.

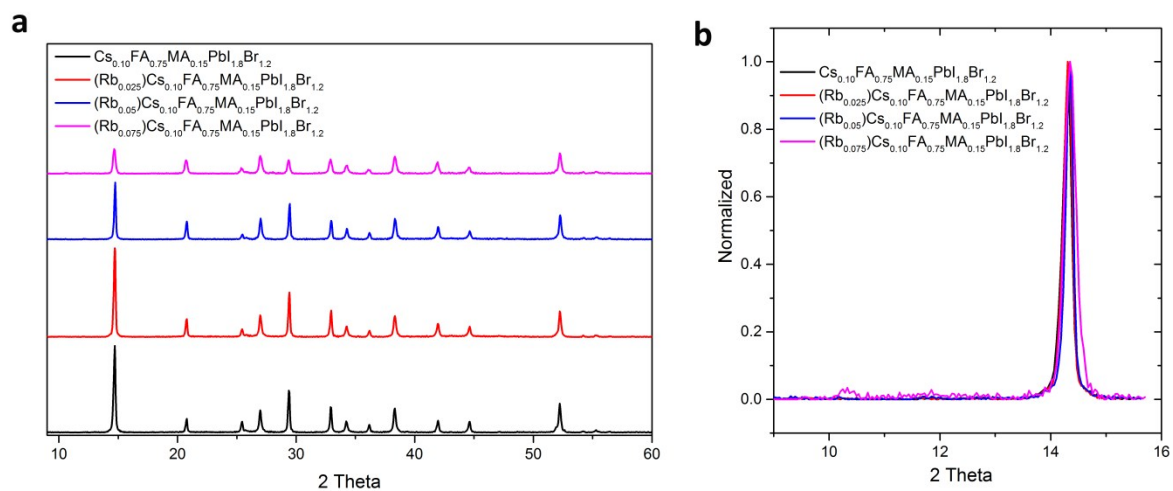


Figure S6. XRD patterns of high bandgap perovskite (1.75 eV) without Rb doping and with Rb doping

The optical property of the perovskite materials is revealed by the transmittance spectra shown in Figure S7 (a), and the bandgap is calculated to be ~ 1.75 eV (inset). The SEM image of the as-prepared perovskite film on top of mesoporous TiO_2 is shown in Figure S7 (b), which is dense without pinholes.

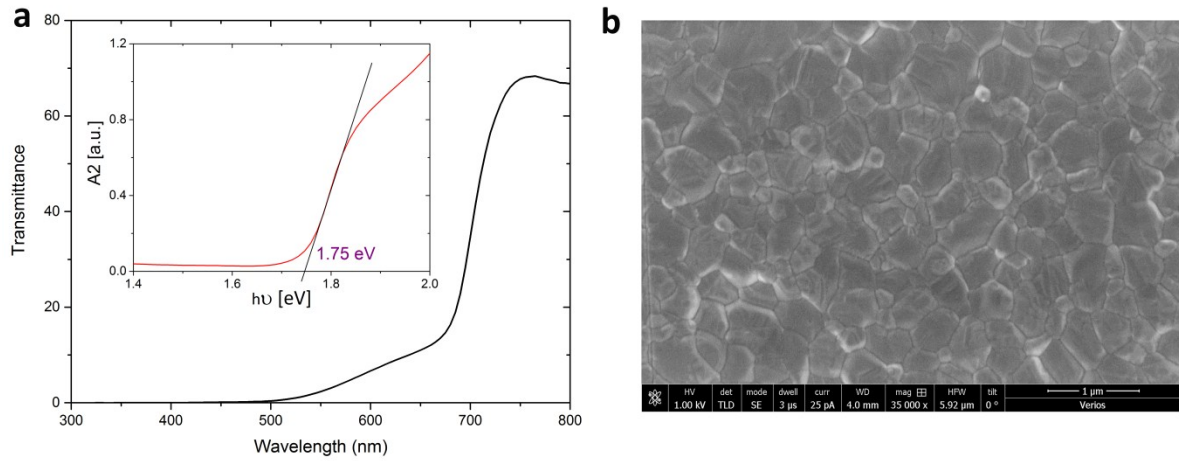


Figure S7. (a) Transmittance spectra and the calculated bandgap of ~ 1.75 eV and (b) SEM image of the $\text{Cs}_{0.1}\text{Rb}_{0.05}\text{FA}_{0.75}\text{MA}_{0.15}\text{Pb}_{1.8}\text{Br}_{1.2}$ film on the FTO/cp-TiOx/ms-TiO₂ layer.

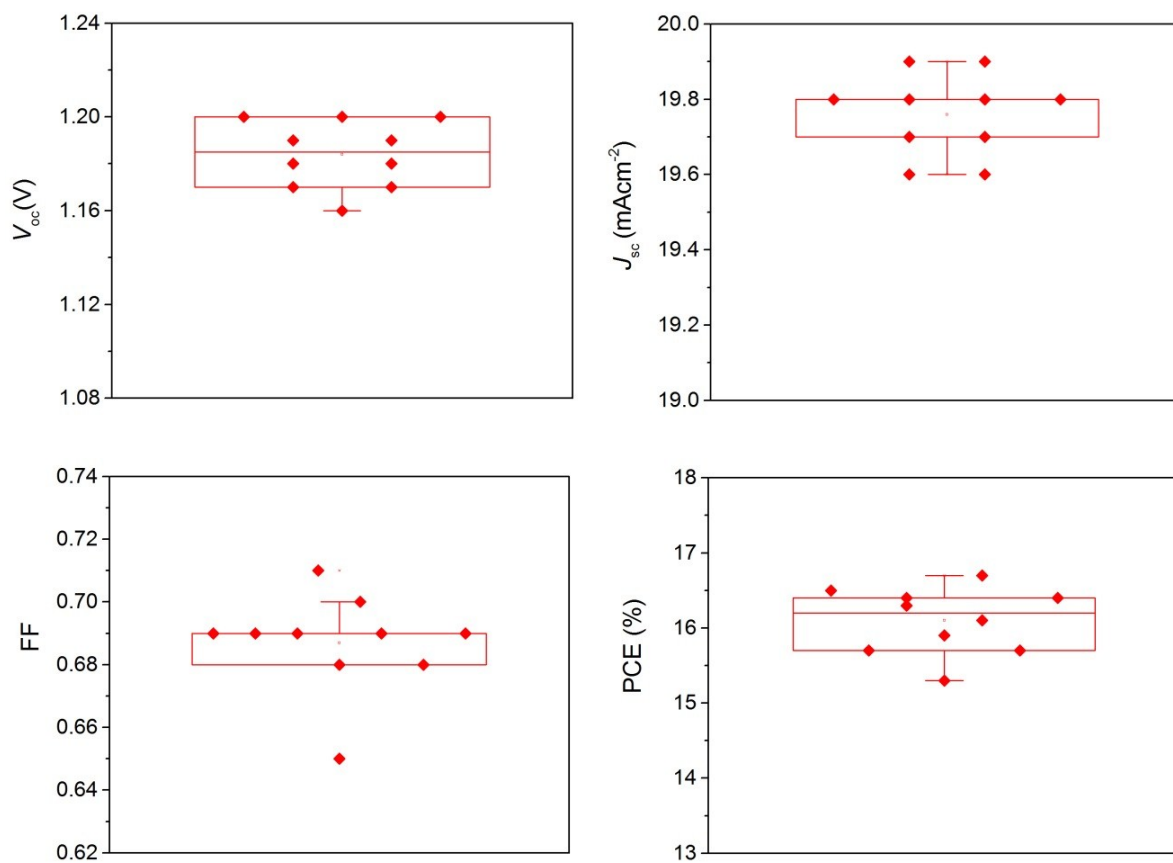


Figure S8. Photovoltaic metrics of ten high bandgap opaque solar cells from two batches based on $\text{Cs}_{0.1}\text{Rb}_{0.05}\text{FA}_{0.75}\text{MA}_{0.15}\text{PbI}_{1.8}\text{Br}_{1.2}$. The average and standard deviation of each photovoltaic parameter are V_{oc} : 1.184 ± 0.014 V; J_{sc} : 19.76 ± 0.11 mAcm^{-2} ; FF: 0.687 ± 0.016 ; PCE: $16.1 \pm 0.44\%$

Similar strategy of optical management was employed in the high bandgap perovskite solar cell. The thickness of MgF_2 on the rear side is ~ 145 nm, which also tunes the optical response in the near-infrared region while induce very small influence for the perovskite solar cell. The current density difference for the high bandgap semi-transparent solar cell with and without MgF_2 is only around 0.2 mAcm^{-2} , corresponding to relative change of $\sim 1\%$. Again, textured foil on the front surface plays dual functions by both enhancing the absorption of the perovskite solar cell in the visible region and the transmittance of perovskite in the long wavelength region.

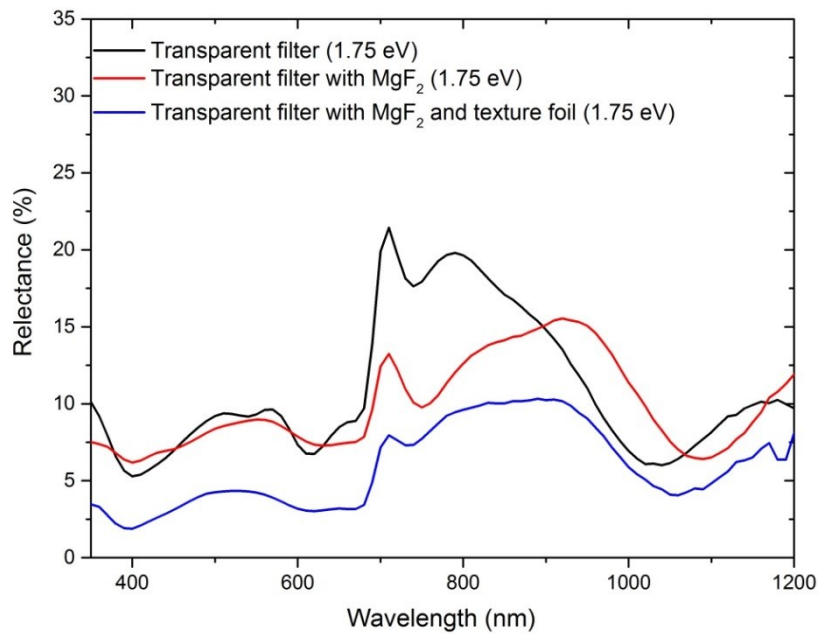


Figure S9. Reflectance of the transparent filters based on high bandgap perovskite ($\text{Cs}_{0.1}\text{Rb}_{0.05}\text{FA}_{0.75}\text{MA}_{0.15}\text{Pb}_{1.8}\text{Br}_{1.2}$) by incorporating MgF_2 on the rear side and texture foil on the front side

EQE of CIGS standalone solar cell with a PCE of 21.7%, and the simulated EQE after filtering with the semi-transparent solar cells developed in this work.

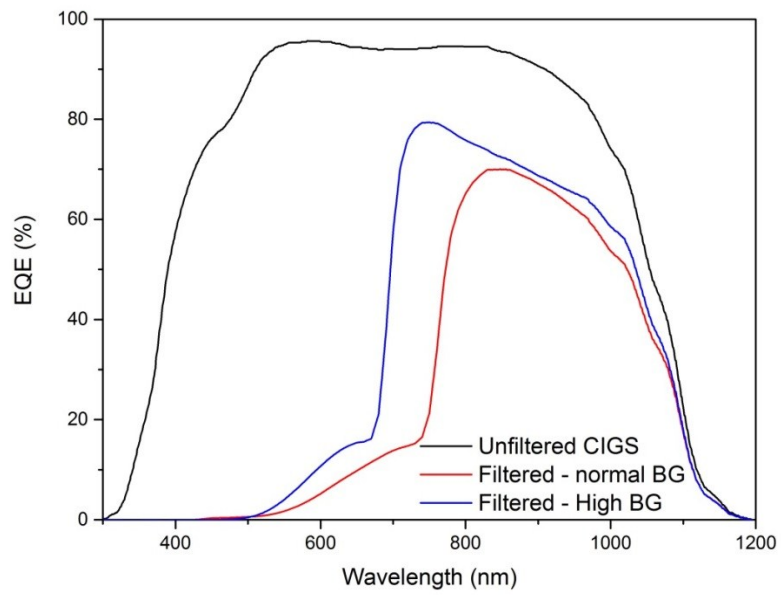


Figure S10. Simulated EQE of CIGS standalone device and those after being filtered with the two different semi-transparent filters developed in this work

XRD patterns of the MAPbI_3 and $\text{Cs}_{0.05}\text{Rb}_{0.05}\text{FA}_{0.765}\text{MA}_{0.135}\text{PbI}_{2.55}\text{Br}_{0.45}$ as fresh and after being exposure to O_2 flow with constant lighth illumination for 5 mins. No change is observed for either perovskite material.

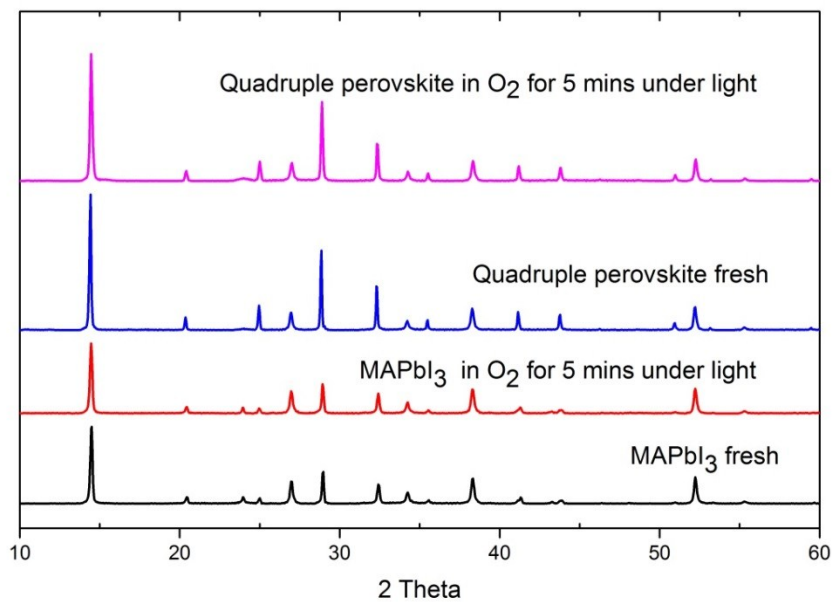


Figure S11. XRD patterns of the MAPbI_3 and quadruple perovskite ($\text{Cs}_{0.05}\text{Rb}_{0.05}\text{FA}_{0.765}\text{MA}_{0.135}\text{PbI}_{2.55}\text{Br}_{0.45}$) as fresh and after being exposed with O_2 under light illumination.

Figure S12 shows the fast J - V curves under N_2 and O_2 by tuning the composition of the perovskite material. The J_{sc} ratio under different atmosphere extracted from these curves for each perovskite condition is summed as Fig. 4 (d).

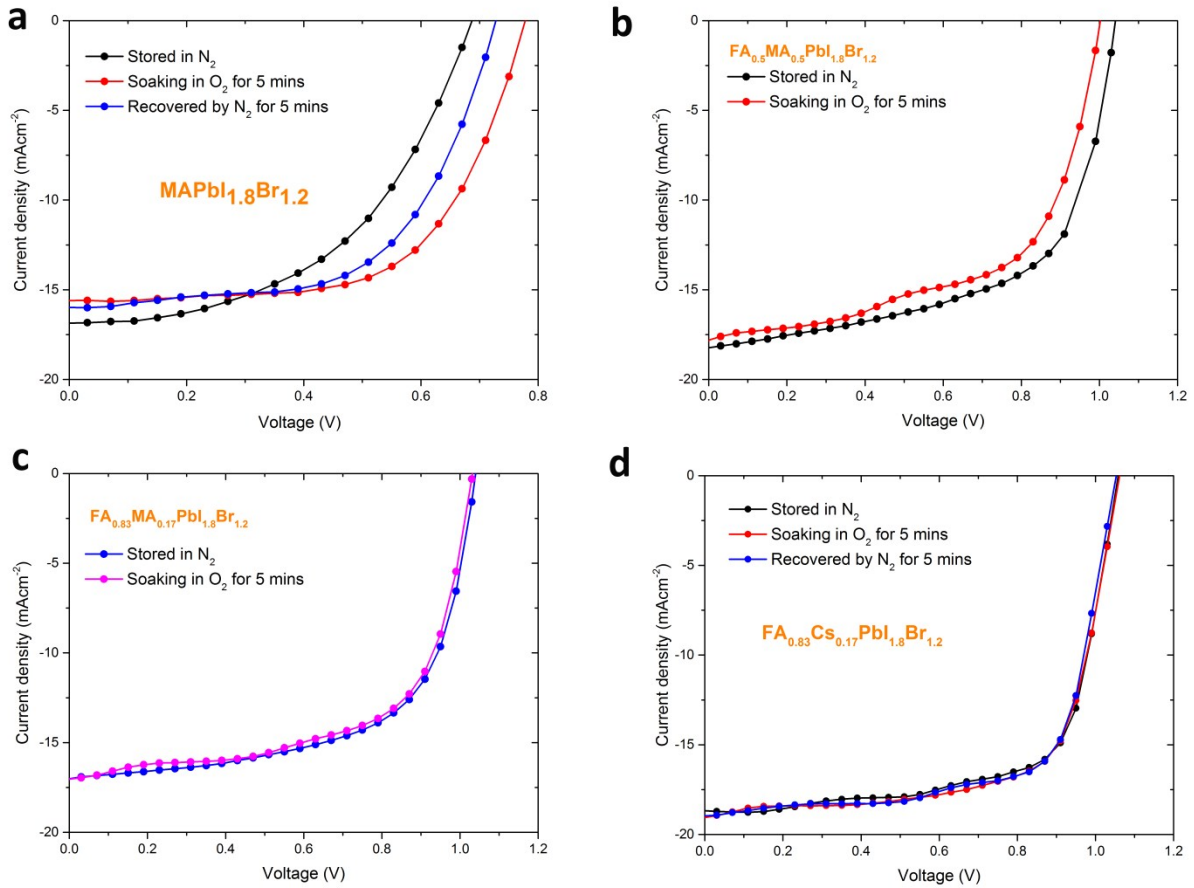


Figure S12. Fast J - V scanning curves of the solar cells based on (a) $\text{MAPbI}_{1.8}\text{Br}_{1.2}$, (b) $\text{FA}_{0.5}\text{MA}_{0.5}\text{PbI}_{1.8}\text{Br}_{1.2}$, (c) $\text{FA}_{0.83}\text{MA}_{0.17}\text{PbI}_{1.8}\text{Br}_{1.2}$ and (d) $\text{FA}_{0.83}\text{Cs}_{0.17}\text{PbI}_{1.8}\text{Br}_{1.2}$

Intriguingly, for MAPbI_{1.8}Br_{1.2} based solar cell, the V_{oc} increases under oxygen exposure (Fig. S13), the reasons for which are not clear at this time. However, this seems to be consistent with the observation that MAPbBr₃ single crystals have previously shown a high sensitivity towards oxygen exposure in the form of oxygen-enhanced photoluminescence[1].

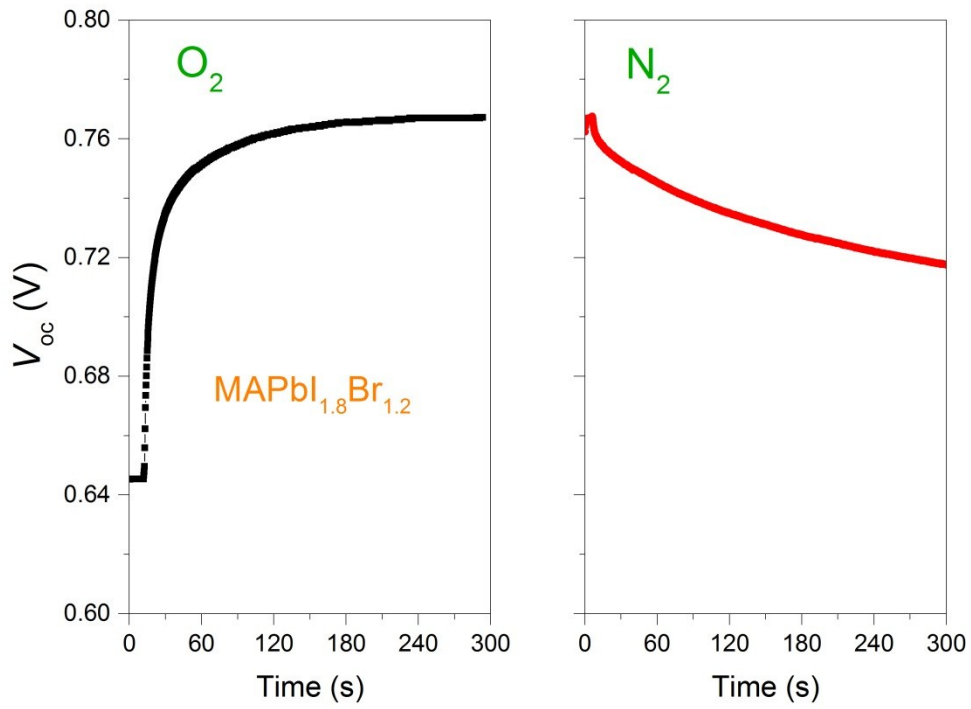


Figure S13. V_{oc} evolution of the device based on MAPbI_{1.8}Br_{1.2}

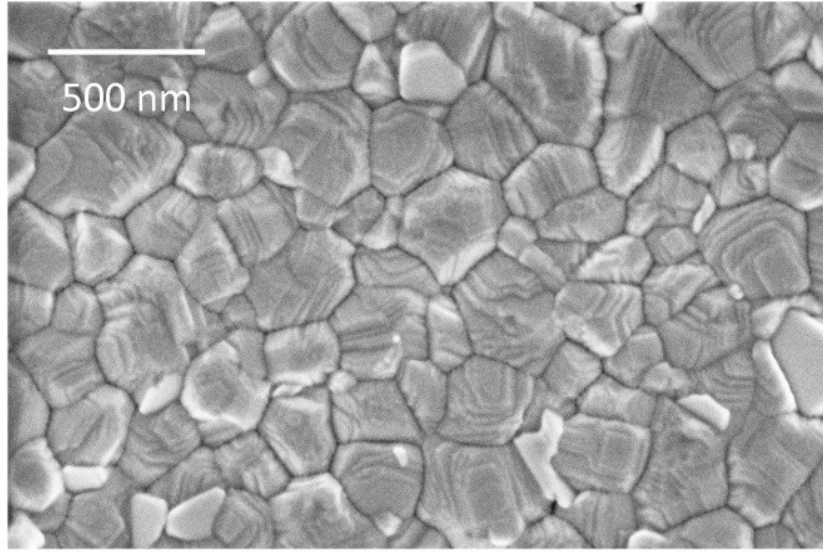


Figure S14. SEM image of MAPbI₃ fabricated by one-step method

The V_{oc} evolutions under N_2 and O_2 for the devices with and without TiO_2 ETM are shown in Fig. S15. Without TiO_2 as electron selective material, the PSC shows unsurprisingly lower V_{oc} . For easy comparison, the V_{oc} is normalized to the maximum data. It is clearly seen that without the TiO_2 ETM, the V_{oc} drop under O_2 is much smaller.

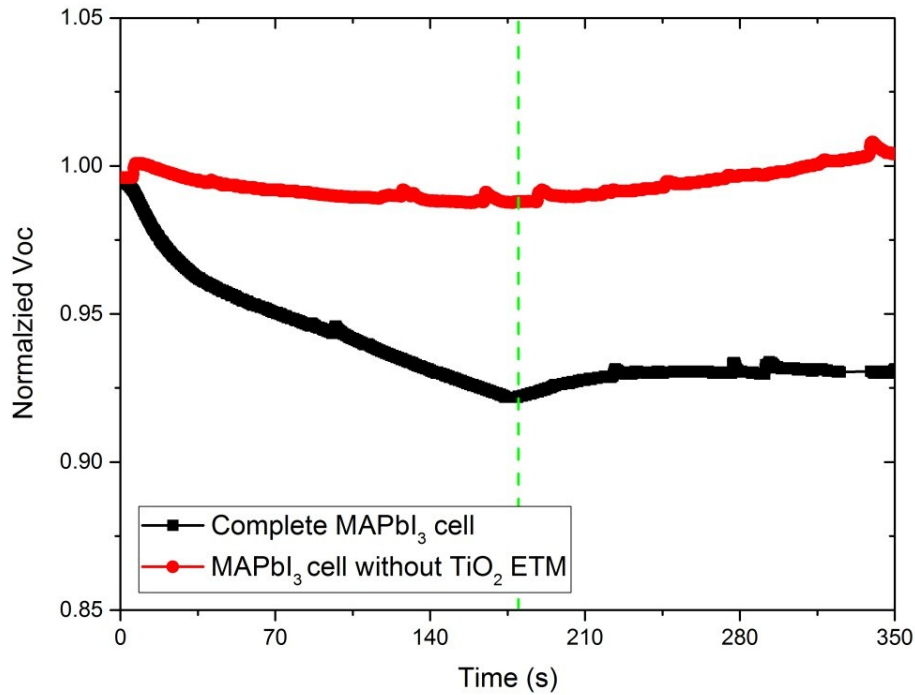


Figure S15. Comparison of V_{oc} evolution of the solar cells based on MAPbI₃ and that without cp-TiO₂/ms-TiO₂ ETM under O_2 and N_2 . The curves on the left side of the dashed green line represent behaviour under O_2 , while the right is after being switching back to N_2 .

Stability of the devices under different conditions based on three perovskite materials were studied and compared. The materials included the widely used MAPbI_3 , and the quadruple perovskite materials of $\text{Cs}_{0.05}\text{Rb}_{0.05}\text{FA}_{0.765}\text{MA}_{0.135}\text{PbI}_{2.55}\text{Br}_{0.45}$ (normal bandgap) and $\text{Cs}_{0.10}\text{Rb}_{0.05}\text{FA}_{0.75}\text{MA}_{0.15}\text{PbI}_{1.8}\text{Br}_{1.2}$ (high bandgap). The devices were not encapsulated. The performance of the devices after being stored in dry air is shown in Fig. S16. Consistent with much reduced sensitivity towards oxygen of the multi-cation perovskite, the as-prepared devices based on quadruple cation perovskites show significantly better stability than that based on MAPbI_3 in dry air. After tracking for 160 h (approximately 7 days), the devices based on $\text{Cs}_{0.05}\text{Rb}_{0.05}\text{FA}_{0.765}\text{MA}_{0.135}\text{PbI}_{2.55}\text{Br}_{0.45}$ and $\text{Cs}_{0.10}\text{Rb}_{0.05}\text{FA}_{0.75}\text{MA}_{0.15}\text{PbI}_{1.8}\text{Br}_{1.2}$ retain $\sim 75\%$ of their original efficiency, while the MAPbI_3 device dropped to $\sim 32\%$ of its original efficiency. We note that cells are exposed to ambient conditions for each efficiency measurement as we need to transfer the sample from the dry cabinet to the home-made jig filled with N_2 . Therefore, the actual stability of these perovskite solar cells could be slightly better if stored in dry conditions continuously.

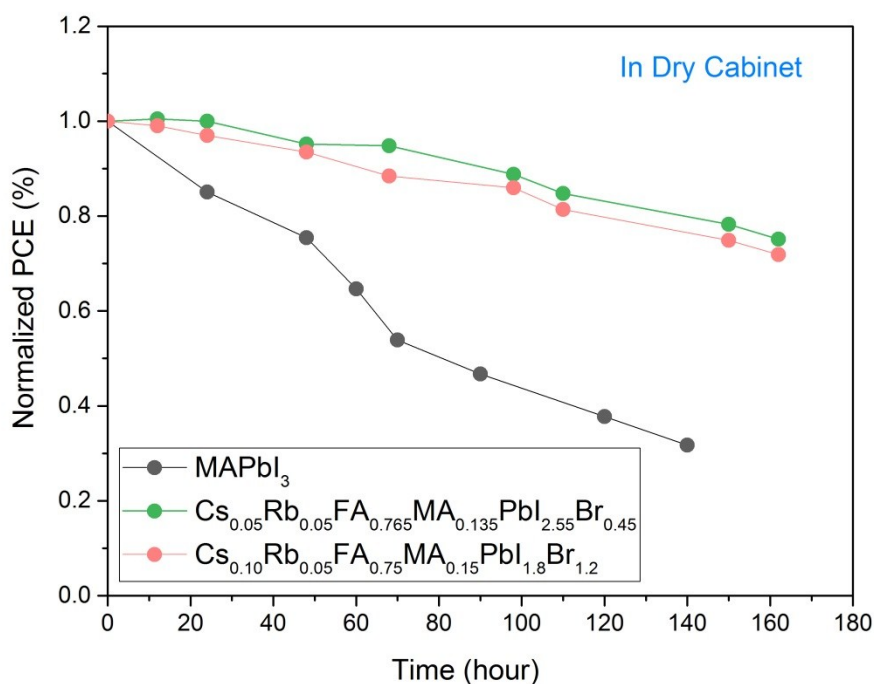


Figure S16. Stability of unencapsulated devices stored under dry air condition (controlled by a drying cabinet) including MAPbI_3 , and the quadruple perovskite materials of $\text{Cs}_{0.05}\text{Rb}_{0.05}\text{FA}_{0.765}\text{MA}_{0.135}\text{PbI}_{2.55}\text{Br}_{0.45}$ (normal bandgap) and $\text{Cs}_{0.10}\text{Rb}_{0.05}\text{FA}_{0.75}\text{MA}_{0.15}\text{PbI}_{1.8}\text{Br}_{1.2}$ (high bandgap)

The effect of the humidity on the unencapsulated perovskite solar cells is evaluated by tracking the efficiency of the devices stored under ambient conditions. The humidity of the ambient conditions is in the range of ~40% - 60% (Fig. S17 (a)). The devices under such condition show much worse stability compared to those stored in the dry air. After around 60 h, the devices based on $\text{Cs}_{0.05}\text{Rb}_{0.05}\text{FA}_{0.765}\text{MA}_{0.135}\text{PbI}_{2.55}\text{Br}_{0.45}$ and $\text{Cs}_{0.10}\text{Rb}_{0.05}\text{FA}_{0.75}\text{MA}_{0.15}\text{PbI}_{1.8}\text{Br}_{1.2}$ only retain around half of their original efficiency, while the MAPbI_3 device efficiency has decreased by ~87%. In comparison, with similar storage time but in dry air, the quadruple perovskite based solar cells retain over 90% of their original efficiency.

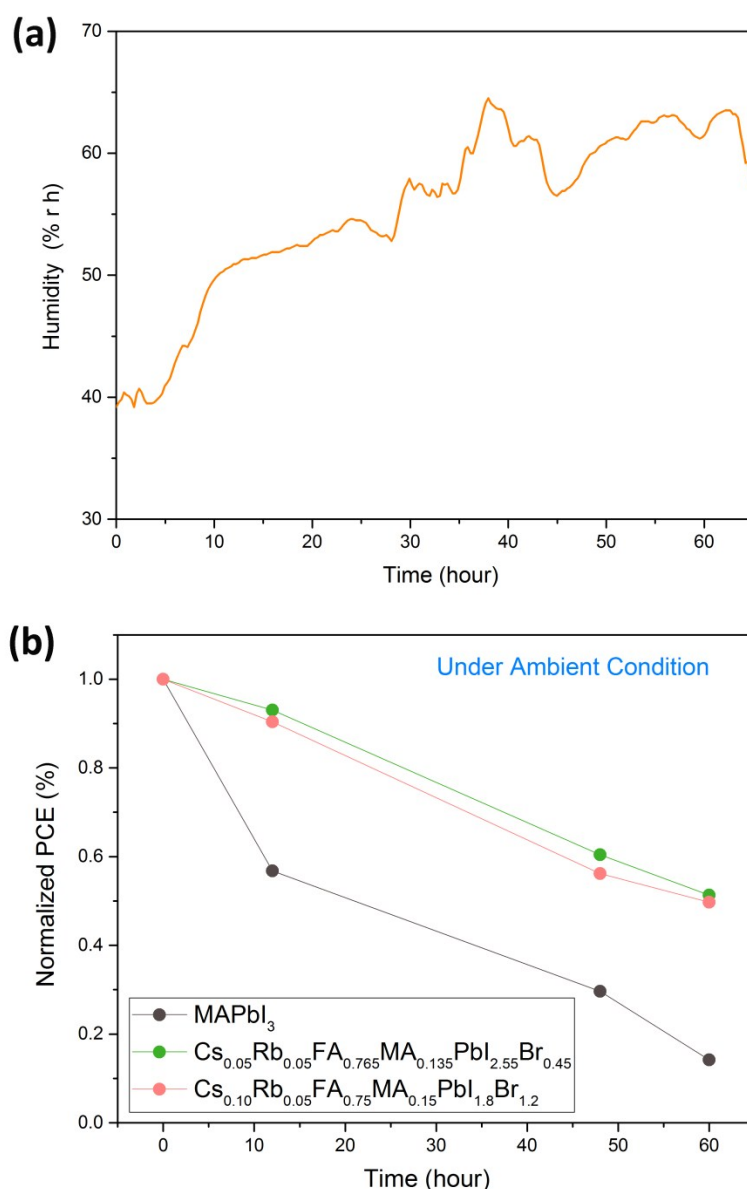


Figure S 17. (a) Track of humidity under the ambient condition. (b) Stability of unencapsulated devices stored under ambient condition including MAPbI_3 , and the quadruple perovskite materials of $\text{Cs}_{0.05}\text{Rb}_{0.05}\text{FA}_{0.765}\text{MA}_{0.135}\text{PbI}_{2.55}\text{Br}_{0.45}$ (normal bandgap) and $\text{Cs}_{0.10}\text{Rb}_{0.05}\text{FA}_{0.75}\text{MA}_{0.15}\text{PbI}_{1.8}\text{Br}_{1.2}$ (high bandgap)

Photos of fresh perovskite solar cells with different compositions and those stored under different conditions are shown in Fig. S18. It is clear that moisture induces more severe degradation for perovskite solar cells than oxygen, especially for MAPbI₃ as revealed by much lighter colour.

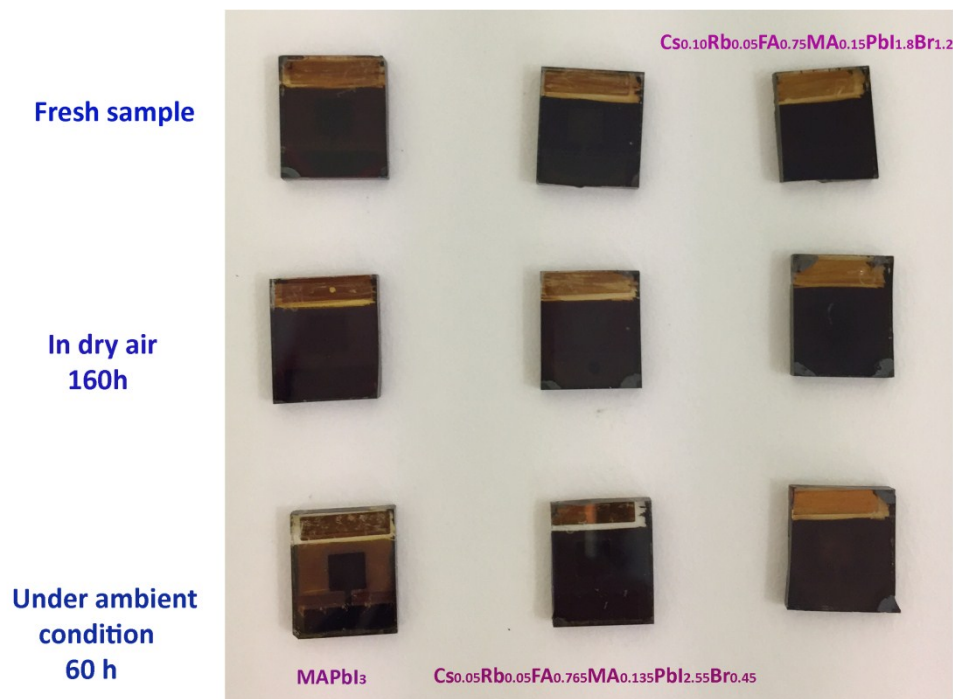


Figure S18. Pictures of as-prepared perovskite solar cells and those stored in different conditions: the devices on the top line are fresh samples, those in the middle are stored in the dry air for 160 h, and those in the bottom are stored under ambient conditions. The three samples on the left are MAPbI₃, those in the middle are devices based on Cs_{0.05}Rb_{0.05}FA_{0.765}MA_{0.135}PbI_{2.55}Br_{0.45}, and the devices on the right are based on the perovskite with a composition of Cs_{0.10}Rb_{0.05}FA_{0.75}MA_{0.15}PbI_{1.8}Br_{1.2}

Eight semi-transparent devices from two batches based on normal bandgap perovskite of $\text{Cs}_{0.05}\text{Rb}_{0.05}\text{FA}_{0.765}\text{MA}_{0.135}\text{PbI}_{2.55}\text{Br}_{0.45}$ have been fabricated and tested. The histogram of each photovoltaic parameter is shown in Fig. S19.

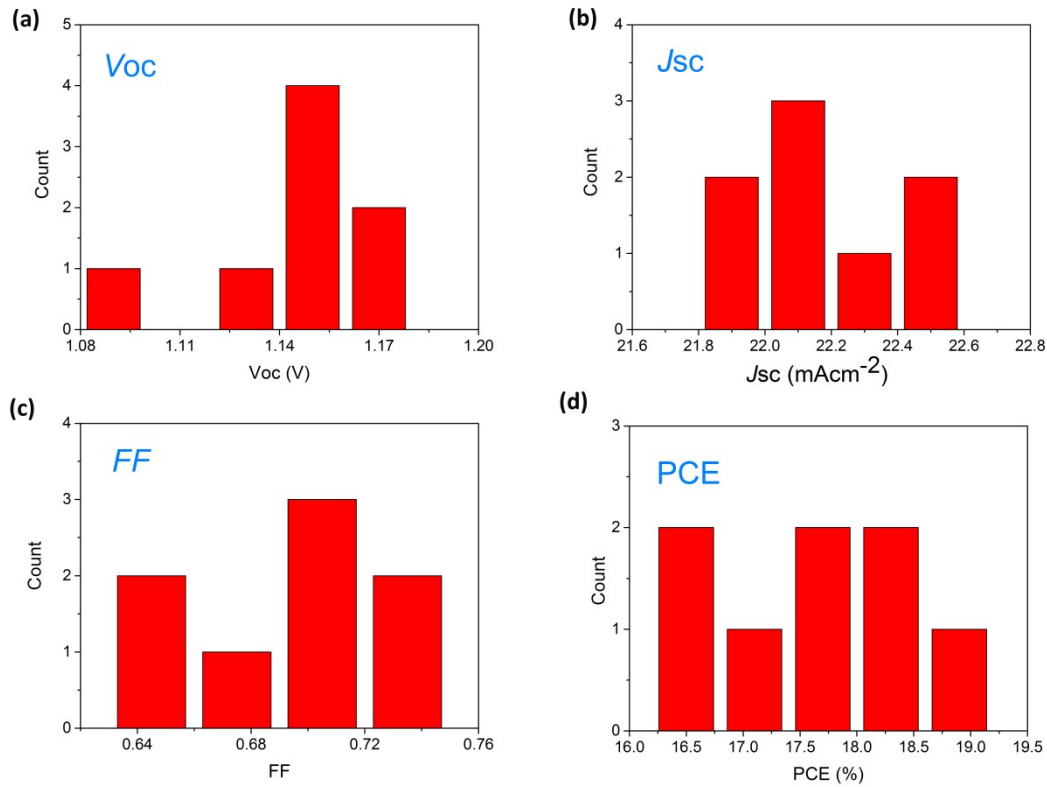


Figure S 19. Histogram of the photovoltaic metrics of eight semi-transparent solar cells from two batches based on normal bandgap of $\text{Cs}_{0.05}\text{Rb}_{0.05}\text{FA}_{0.765}\text{MA}_{0.135}\text{PbI}_{2.55}\text{Br}_{0.45}$. The average and standard deviation of each photovoltaic parameter are V_{oc} : 1.139 ± 0.024 V; J_{sc} : 22.16 ± 0.23 mAcm^{-2} ; FF: 0.694 ± 0.035 ; PCE: $17.5 \pm 0.9\%$.

Eight semi-transparent devices from two batches based on high bandgap perovskite of $\text{Cs}_{0.10}\text{Rb}_{0.05}\text{FA}_{0.75}\text{MA}_{0.15}\text{PbI}_{1.8}\text{Br}_{1.2}$ have been fabricated and tested. The histogram of each photovoltaic parameter is shown in Fig. S19.

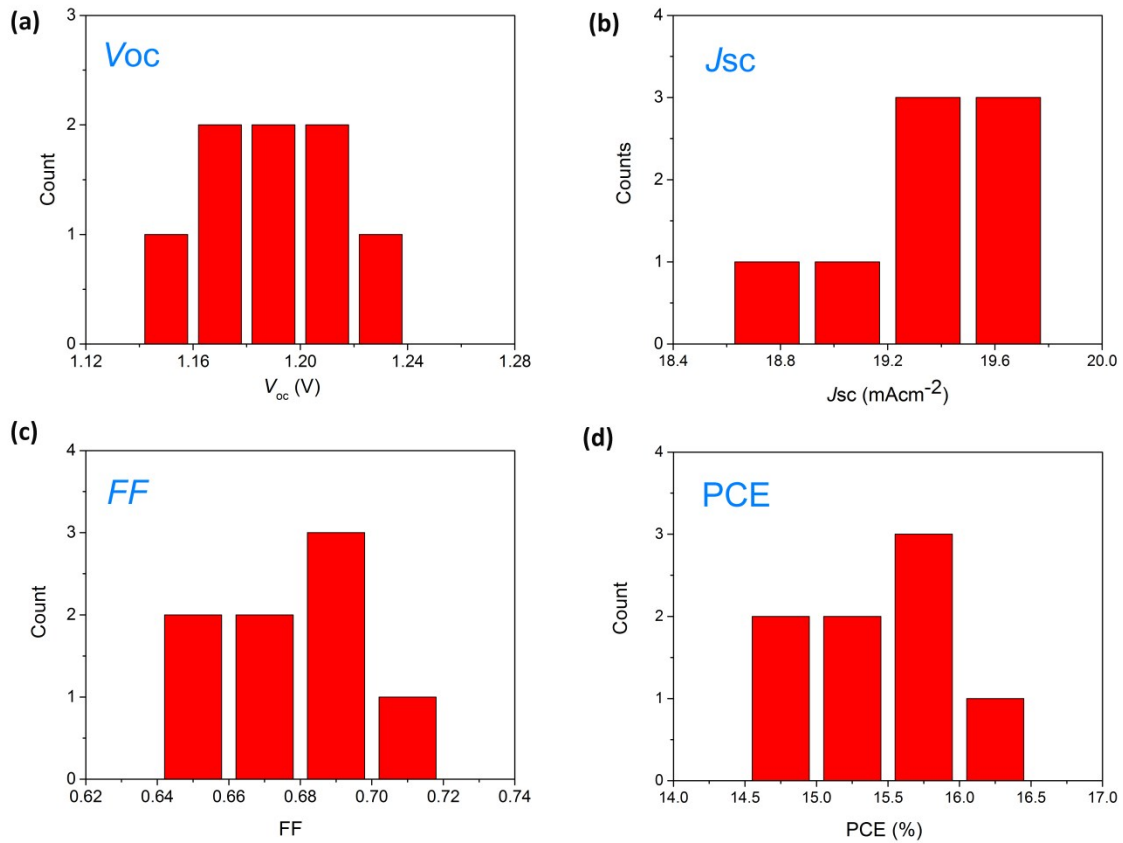


Figure S20. Histogram of the photovoltaic metrics of eight semi-transparent solar cells from two batches based on high bandgap perovskite of $\text{Cs}_{0.10}\text{Rb}_{0.05}\text{FA}_{0.75}\text{MA}_{0.15}\text{PbI}_{1.8}\text{Br}_{1.2}$. The average and standard deviation of each photovoltaic parameter are V_{oc} : 1.188 ± 0.028 V; J_{sc} : 19.3 ± 0.33 mAcm^{-2} ; FF: 0.673 ± 0.024 ; PCE: $15.3 \pm 0.6\%$.

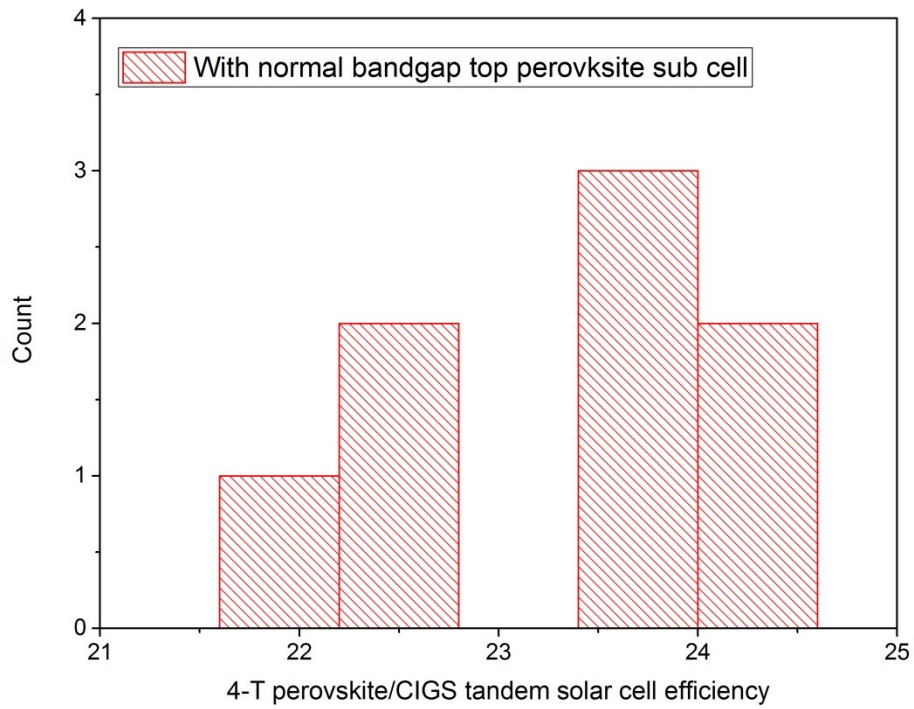


Figure S21. Histogram of the efficiency of 4-T perovskite/CIGS tandem solar cell based on normal bandgap perovskite top subcell. The average and standard deviation of the efficiency is: $23.3 \pm 0.9\%$.

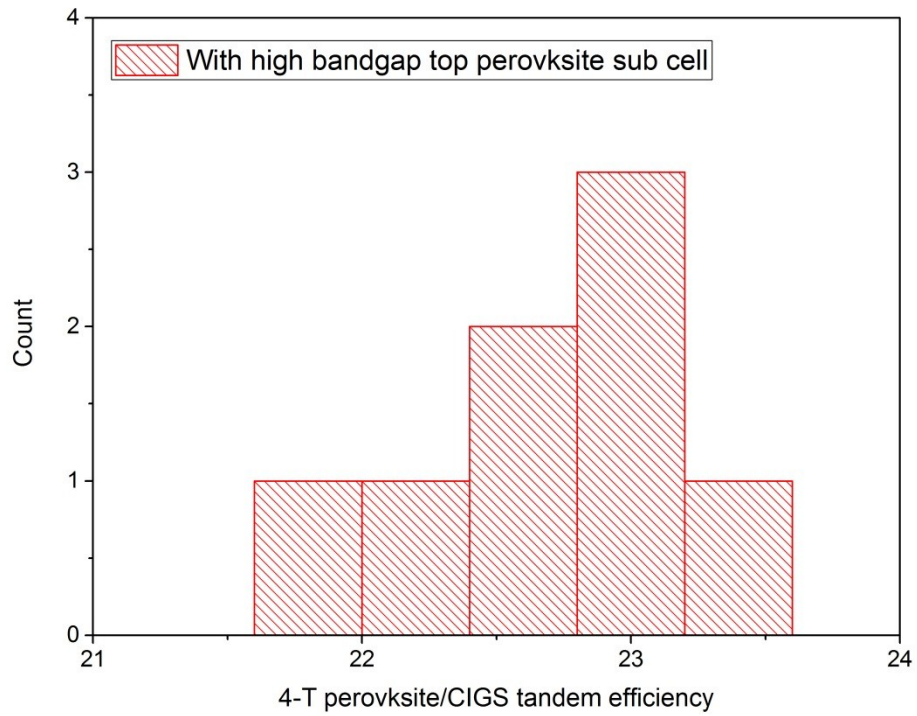


Figure S22. Histogram of the efficiency of 4-T perovskite/CIGS tandem solar cell based on high bandgap perovskite top subcell. The average and standard deviation of the efficiency is: $22.7 \pm 0.6\%$.

1. H.-H. Fang, S. Adjokatse, H. Wei, J. Yang, G.R. Blake, J. Huang, J. Even, M.A. Loi, *Science Advances*, 2016. **2**(7).